Journal of Materials Chemistry A

Accepted Manuscript

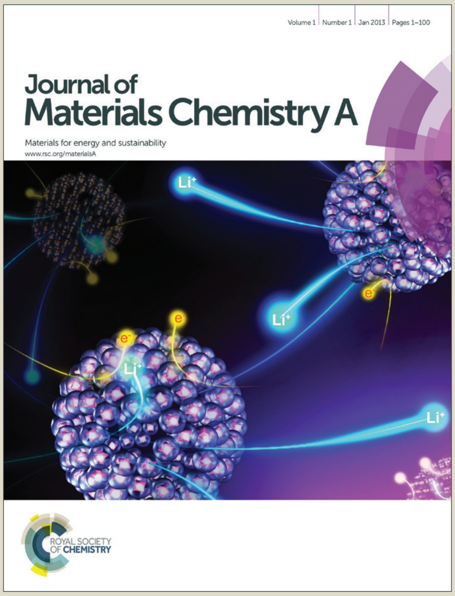

ROYAL SOCIETY OF CHEMISTRY

www.rsc.org/materialsA

Lithiation/Delithiation Mechanism of Monodispersed MSn_5 (M=Fe, Co and FeCo) Nanospheres

Fengxia Xin,[a] Xiaoliang Wang,[b] Jianming Bai,[c] Wen Wen,[d] Huajun Tian,[a] Chunsheng Wang,[e,]* and Weiqiang Han[a,]*

[a]*Ningbo Institute of Materials Technology & Engineering, Chinese Academy of Sciences, Ningbo, 315201, P. R. China*

[e]*Department of Chemical and Biomolecular Engineering University of Maryland College Park, MD 20742, USA*

[b]*Present address: Seeo Inc., 3906 Trust Way, Hayward, CA 94545*

[c]*National Synchrotron Light Source, Brookhaven National Laboratory, Upton, New York 11973, United States*

[d]*Shanghai Synchrotron Radiation Facility, Shanghai Institute of Applied Physics, Chinese Academy of Sciences, Shanghai 201204, P. R. China*

Corresponding Author:

E-mail: hanweiqiang@nimte.ac.cn, *cswang@umd.edu*

Abstract

Designed Sn based alloy host as a higher capacity and longer cycle life for next generation lithium-ion battery, monodisperse nanospheres of intermetallic MSn_5 (M=Fe, Co and FeCo) phase were synthesized by nanocrystal conversion chemistry method using preformed Sn nanospheres as templates. The same crystal structure, identical particle surface morphology and the similar particle size distribution (30~50 nm) of these intermetallic MSn_5 (M=Fe, Co and FeCo) phase are ideal for comparison on the electrochemical performance, reaction mechanism, thermodynamics and kinetics during lithiation/delithiation. Importantly, MSn_5 (M=Fe, Co and FeCo) phase with defect structure $Fe_{0.74}Sn_5$, $Co_{0.83}Sn_5$ and $Fe_{0.35}Co_{0.35}Sn_5$, exhibit the highest theoretical capacity of > 917 mAh g^{-1} among the reported M-Sn (M is electrochemically inactive) based intermetallic anodes. The ex situ XRD and XAFS illustrate the complete reversibility of MSn_5 (M=Fe, Co and FeCo) phase during lithium insertion/extraction for the first cycle. $Fe_{0.35}Co_{0.35}Sn_5$ anode can take advantages of both high capacity of $Fe_{0.74}Sn_5$ and long cycle life of $Co_{0.83}Sn_5$, providing 736 mAh g^{-1} and maintaining 92.7% of initial capacity after 100 cycles with an average capacity loss of only 0.07% per cycle. The excellent electrochemical performance of $Fe_{0.5}Co_{0.5}Sn_5$ system is attributed to higher reversibility, lower reaction resistance. This work provides a novel insight toward designing and exploring optimal Sn based alloy anode for next generation Li-ion batteries.

1. Introduction

Rechargeable lithium-ion batteries have attracted much attention because they have been widely used in mobile communication devices, portable electronic devices, and may play a critical role in emerging electric vehicles (EV) and large-scale renewable energy storage.[1-3] To satisfy the high energy requirement of EV, substantial improvements in energy density of current Li-ion batteries are requested. One of the promising electrode materials that can potentially meet these requirements is M (electrochemically inactive)-Sn intermetallics materials, which have the advantage of high theoretical mass capacity and volumetric capacity than that of the state-of-the-art graphite anodes (372 mAh g^{-1} and 883 mAh cm^{-3}).[4-10] Most importantly, the beneficial role of M is to offer a "buffer zone" to compensate the volume fluctuation during lithiation/delithiation, which avoids the pulverization or aggregation of the Sn particles, stabilizes solid electrolyte interphase (SEI) and thus improves the cycling stability.[11-15]

Among M-Sn intermetallics, considerable effort has been devoted to develop high capacity Fe-Sn, Co-Sn, Fe-Co-Sn systems in the academic and industry.[4, 16-20] Recently, our research group has synthesized nonequilibrium $Fe_{0.74}Sn_5$ and $Co_{0.83}Sn_5$ new intermetallic compounds with the theoretical capacity of 929, 918 mAh g^{-1} respectively, which is different from Mike Thackeray's patent and has the highest capacity to date among the reported Sn-based binary intermetallic anodes.[21, 22] Although $Fe_{0.74}Sn_5$ and $Co_{0.83}Sn_5$ share the same crystal structure, their electrochemical performance is quite different. $Fe_{0.74}Sn_5$ has high capacity of 750 mAh g^{-1}, but poor cycle life,[21] while $Co_{0.83}Sn_5$ has long cycling stability but low capacity (500 mAh g^{-1}).[22] Due to lack of knowledge on the lithiation/delithiation mechanism of $Fe_{0.74}Sn_5$ and $Co_{0.83}Sn_5$, the difference of electrochemical performance between them and the effect of M (Fe, Co) element in the alloy are not fully understood. Since the electrochemical performance of MSn_5 (M=Fe, Co and FeCo) are very sensitive to particle size and the crystal structure, the comparison study on the electrochemical performance and reaction mechanism of MSn_5 (M=Fe, Co and FeCo) should be conducted using MSn_5 with the identical particle size, structure and morphology.[23] However, it is very difficult to synthesize $FeSn_5$, $CoSn_5$, $Fe_{0.5}Co_{0.5}Sn_5$ intermetallics phases with the identical structure, composition and particle size using traditional synthesis techniques (such as chemical vapor deposition,[24] electroplating,[25-27] ball milling,[28, 29] carbothermal reduction[30] and arc-melting[31, 32]) due to the large difference of melting point between Sn and Co, Fe. Nanocrystal conversion chemistry promotes compositional and morphological attributes on final products, which is a powerful approach for synthesis of homogeneous nano-sized materials with well-defined shapes and structure.[33-36]

Since MSn_5 (M=Fe, Co and FeCo) phases with defect structure $Fe_{0.74}Sn_5$, $Co_{0.83}Sn_5$ and $Fe_{0.35}Co_{0.35}Sn_5$ are currently absent in the equilibrium Fe-Sn, Co-Sn, Fe-Co-Sn phase diagram and have the highest theoretical capacity of 929, 918, 931 mAh g^{-1} among the reported M (M is electrochemically inactive)-Sn intermetallic anodes, in this work, we have successfully synthesized $FeSn_5$, $CoSn_5$ and $Fe_{0.5}Co_{0.5}Sn_5$ intermetallic phases with same crystal structure, identical particle surface morphology and the similar particle distribution (30~50 nm) from the same Sn nanoparticle templates using unique nanocrystal conversion chemistry method. Moreover, we systemically investigated the lithiation/delithiation reaction mechanism of MSn_5 (M=Fe, Co and FeCo), and compared the reaction thermodynamics, reaction kinetics and electrochemical performance among these three compounds. The insight obtained from this work also provides guidance for the design of other Sn-based compounds for next generation Li-ion batteries.

2. Experimental Section

2.1 Chemicals and Synthesis

Tin (II) chloride ($SnCl_2$, anhydrous, 99%, Alfa), Iron(III) chloride ($FeCl_3$, anhydrous reagent grade, 97%, Aldrich), Cobalt(II) chloride hexahydrate ($CoCl_2{\cdot}6H_2O$, 99.9% metal basis, Alfa), polyvinylpyrrolidone (PVP, MW=360 000, Aldrich), and poly(2-ethyl-2-oxazoline) (PEtOx, MW=50 000, Alfa), tetraethylene glycol (TEG, 99%, Alfa) and sodium borohydride ($NaBH_4$, 98%, Alfa) were used as starting materials.

The preparation of $Fe_{0.5}Co_{0.5}Sn_5$ nanospheres was carried out under an argon atmosphere via a Schlenk line following the procedure developed by Chou et al. First, 30-50 nm tin nanospheres were synthesized in a three necked flask and used it as a template to obtain $Fe_{0.5}Co_{0.5}Sn_5$. As surface stabilizers, 1.57 g of PVP and 0.66 g of PEtOx were added into 35 mL of TEG. After the mixture was totally dissolved in TEG after vigorously stirring at the temperature of 170^{o}C, a 0.3 g of $SnCl_2$ was added into 4 mL of PVP-PEtOx-TEG. After dropping of 0.6 g $NaBH_4$ as a reducing agent for 15 min, tin nanospheres were precipitated turning the suspensions solution from colorless to turn black. To synthesize $Fe_{0.5}Co_{0.5}Sn_5$ nanospheres from tin nanosphere template, the temperature of the suspensions was increased to 200 °C under argon, $FeCl_3$ and $CoCl_2$ solution (0.01930 g of $FeCl_3$ and 0.0094g of $CoCl_2{\cdot}6H_2O$ in 8 mL of TEG) was injected into tin nanosphere suspension drop by drop until the molar ration of (Fe+Co) to (Sn) reach to 0.1. After 1.5 hours at 200°C, the samples were cooled down to room temperature, $Fe_{0.5}Co_{0.5}Sn_5$ nanospheres were harvested by centrifugation and washed with ethanol for several times before drying under vacuum overnight. The $FeSn_5$ and $CoSn_5$ nanospheres were synthesized through a similar conversion chemistry process.[21, 22]

2.2 Structural characterization

The synchrotron powder X-ray diffraction (XRD) pattern were performed using beamline BL14B1 (λ =1.2398 Å) of the Shanghai Synchrotron Radiation Facility

(SSRF) with a NaI point detector at a step rate of 0.02 degrees. The XRD patterns of the materials were analyzed using the software Jade 6.5(Materials Data Incorporated), Jana 2006 (Petricek, V., Dusek, M., and Palatinus, L., 2006), and Superflip. The lattice parameters were obtained by fitting the XRD data using software TOPAS-Academic V4.1 (Coelho Software, Brisbane, 2007). The Sn K-edge XAFS spectras were collected in transmission mode at beamline BL14W using Si (311) detector. Reference spectrum of Sn element for the energy calibration was simultaneously collected with the corresponding Sn metal foils. The samples were characterized using scanning electron micros-copy (FESEM and HR-SEM, Hitachi, S-4800) using an operating voltage of 8 kV and transmission electron microscopy (TEM, Tecnai F20 and JEOL 2100) with an energy dispersive X-ray spectroscopy (EDS) detector.

2.3 Electrochemical Measurements

The work electrode films were composed of the active materials, carbon black and binder with the weight composition of 80: 10: 10 on copper foils. The active material loading weight was ~0.5 mg/cm^2 and the films were dried in a vacuum oven at 110°C overnight. Lithium foil served as both the counter and reference electrodes under ambient temperature. Carbon black (Super P) is from TIMCAL, and sodium carboxymethyl cellulose (CMC, MW∼ 90 000) binder is from Alfa Aldrich. The Celgard 2320 membrane was used as the separator and Li metal as a counter and a reference electrode. 1.0 M solution of $LiPF_6$ in ethylene carbonate/dimethyl carbonate/ethyl methyl carbonate (EC/DMC/EMC, 1:1:1 in volume (CAPCHEM) was used as the electrolyte solution. The 2032-type coin cells were fabricated in an argon-filled glove box with both moisture and oxygen contents below 0.1 ppm. All galvanostatic charging/discharging and GITT tests were conducted on a multichannel battery-testing system (BT2000, Arbin Instruments, USA) with the voltage range of 0.01-1.5 V in room temperature at the current rate of C/20 (i.e., the time for full charge or discharge of the theoretical capacity was 20 h). Cyclic voltammetry (CV) between 0.01 and 2 V at a scan rate of 0.02 mV/s and EIS of anodes were recorded using an electrochemical workstation (1470E, UK).

3. Results and Discussion

3.1 Materials synthesis and characterizations

Monodisperse $FeSn_5$, $Fe_{0.5}Co_{0.5}Sn_5$ and $CoSn_5$ nanospheres were obtained by using Sn nanospheres as templates. The formation mechanism of MSn_5 (M=Fe, Co and FeCo) nanospheres is shown in **Fig. 1**a, and illustrated in detail in Experimental Section. The similar particle distribution (30~50 nm) of these three compounds is demonstrated using electron microscope images in **Fig. 1**b, **1**e, **1**h. Moreover, the high-resolution transmission electron microscopy (HRTEM) images revealed that all $FeSn_5$, $Fe_{0.5}Co_{0.5}Sn_5$, $CoSn_5$ nanospheres had core−shell structure consisting of a ~30 nm single-crystalline intermetallic core and a ~4 nm amorphous oxide shell (**Fig. 1**c, **1**f, **1**i). The STEM EDS elemental mapping images in **Fig. 1**d, **1**g, **1**j clearly demonstrated that transition metals (Fe or Co) and Sn in the nanospheres were homogeneous distributed. Moreover, the ratios of Sn to transition metal are about 7:1, 7:1, and 6:1 for the Sn/Fe, Sn/Fe+Co and Sn/Co respectively as evidenced by transmission electron microscopy energy dispersive X-ray spectroscopy (TEM-EDS). The ratio deviation from 5:1 in MSn_5 indicated the existence of Co/Fe vacancies in $FeSn_5$, $Fe_{0.5}Co_{0.5}Sn_5$, $CoSn_5$ phase,[21] which nonstoichiometry always existed in alloy materials.[37-39]

Since MSn_5 did not exist in equilibrium diagram, we characterized the detailed structures of three MSn_5 compounds using synchrotron powder X-ray diffraction (XRD) patterns (**Fig. 2**a). The crystal structures including refined lattice parameters, thermal factors, atomic coordinates, occupancies, d spacing, and relative intensity were resolved by the charge-flipping method. The $FeSn_5$, $Fe_{0.5}Co_{0.5}Sn_5$, $CoSn_5$ nanospheres from the β-Sn nanosphere template were chemically pure with highly crystalline tetragonal phase in the P4/mcc space group. With increasing the proportion of Fe from $CoSn_5$, $Fe_{0.5}Co_{0.5}Sn_5$, to $FeSn_5$, a and b axis were slightly reduced (summarized in **Table S1**). Meantime, the lattice parameter c was elongated by 1.68%

in comparison with the original phase due to the volume expansion from phase $CoSn_5$ (278.8 $Å^3$) to $FeSn_5$ (281.5 $Å^3$) because the crystal radius of Fe is a little lager than that of Co. The refine analysis demonstrated that the Fe and Co atoms partially occupied the 2c sites in $FeSn_5$, $Fe_{0.5}Co_{0.5}Sn_5$, $CoSn_5$ phase, revealing the existence of vacancies, which were also evidenced by TEM-EDS. Accordingly, the real compositions of these nanospheres are $Fe_{0.74}Sn_5$, $Fe_{0.35}Co_{0.35}Sn_5$ and $Co_{0.83}Sn_5$. **Fig. 2**b shows a representative set of Fourier transforms (FTs) of the synchrotron X-ray absorption fine structure (XAFS) spectra at the Sn K-edge, which confirmed that $Fe_{0.74}Sn_5$, $Fe_{0.35}Co_{0.35}Sn_5$ and $Co_{0.83}Sn_5$ had the same MSn_5 structure. The Sn atoms in these samples formed the first coordination shell, with a Sn−Fe (Co) bond length, and Sn and Sn atoms formed the second coordination shell similar to that in Sn foil.

3.2 Electrochemical performance of $FeSn_5$, $Fe_{0.5}Co_{0.5}Sn_5$ and $CoSn_5$ nanospheres

As far as we know, intermetallic $FeSn_5$, $CoSn_5$ and $Fe_{0.5}Co_{0.5}Sn_5$ phases with the defect structure ($Fe_{0.74}Sn_5$, $Co_{0.83}Sn_5$ and $Fe_{0.35}Co_{0.35}Sn_5$) have the highest theoretical capacity of 929, 918 and 931 mAh g^{-1} among the reported M-Sn (M is electrochemically inactive) binary and ternary intermetallic anodes.[21] The charge/discharge behaviors of the three MSn_5 anodes at 0.05 C between 0.05 V and 1.5 V in the 1, 2 and 5 cycles are shown in **Fig. 3**(a-c). All three MSn_5 cathodes show similar lithiation/delithiation behaviors. The plateau at 0.7 V and 1.3-1.7 V in the first lithiation were associated with the reduction of amorphous Sn oxide shell and electrolyte decomposition on the surface of the nanospheres, resulting in the irreversible discharge capacity.[40, 41] In the following lithiation cycles, the voltage plateaus at 1.3-1.7 and at 0.7 V dispersed and the voltage profile shifted to left. The delithiation profiles mainly exhibited 2 plateaus at ~0.5 V and ~0.65 V, as well as a slanted plateau above 0.75 V. The detailed lithiation/delithiation behavior of $FeSn_5$, $Fe_{0.5}Co_{0.5}Sn_5$, $CoSn_5$ nanospheres were investigated using cyclic voltammetry (CV) measurement using lithium as the reference/counter electrode. The CV curves of three MSn_5 anodes in the first five cycles measured at a scan rate of 0.02 mV/s between 0.01 V and 2.0 V are shown in **Fig. S1**. During the first lithiation, there were two broad cathodic peak at around 1.7 V and 1.3 V which could be attributed to the formation of solid-electrolyte interface (SEI) films and/or the irreversible lithiation of the surface oxidized layer,[42] since these two peaks disappeared in the following lithiation. A-broad-peak centered at 0.3 V and a-small-peak centered at 0.55 V was associated with the phase change in the alloy process. In the delithiation process, three broad oxidation peaks at around 0.47 V, 0.63 V and 0.75 V corresponded to the reversible phase change in the de-alloying process. The CV curves were in good agreement with the charge/discharge curves.

Fig. 3d illustrates the cycling stability of $FeSn_5$, $Fe_{0.5}Co_{0.5}Sn_5$, $CoSn_5$ nanospheres upon cycling at 0.05 C rate. $Fe_{0.74}Sn_5$ could deliver a high capacity of ~750 mAh g^{-1}, but the capacity quickly dropped after 15 cycles. On the other hand, $Co_{0.83}Sn_5$ nanospheres had only a capacity of 500 mAh g^{-1} but it could maintain similar capacity for 100 cycles. The $Fe_{0.35}Co_{0.35}Sn_5$ had both high capacity as $Fe_{0.74}Sn_5$ and long cycling stability as $Co_{0.83}Sn_5$. The capacity of $Fe_{0.35}Co_{0.35}Sn_5$ increased with initial cycles to 736 mAh g^{-1} at cycle 25, and maintained 92.7% of initial capacity after 100 cycles. The average capacity loss was only 0.07% per cycle. The increase in cycle capacity early in the cycling of the $Fe_{0.35}Co_{0.35}Sn_5$ may be due to: (i) the formation and stabilization of the SEI; (ii) an activation process of electrode (especially for high capacity electrodes with large volume changes) in initial few lithium uptake/removal cycles;[43] (iii) the improvement of Li insertion/extraction kinetics. Given the almost identical crystal structure and nanostructure, this significant difference in cell performance could be closely tied to the difference in composition (i.e., Fe and Co). Based on these findings, the presence of Fe could lead to high capacity, while the presence of Co resulted in superior stability.

Further, the lithiation and delithiation mechanisms of three MSn_5 compounds were investigated using ex situ X-ray diffraction (XRD) and X-ray absorption fine structure (XAFS). The phase evolution at different lithiation and delithiation levels marked in the first charge/discharge curves (a-g, a'-g', a"-g" in **Fig. 4**a, **4**d, **4**g) were identified using ex situ XRD and XAFS. The ex situ XRD patterns at marked lithiation/delithiation levels in **Fig. 4**a, **4**d and **4**g are shown in **Fig. 4**b, **4**e, **4**h respectively. The XAFS at the corresponding lithiation/delithiation levels are shown in **Fig. 4**c, **4**f and **4**i. At open circuit potential (a, a', a"), XRD patterns could be indexed to the tetragonal structure $FeSn_5$, $Fe_{0.5}Co_{0.5}Sn_5$ and $CoSn_5$ in the P4/mcc space group. The Sn amorphous oxides layer could not be detected by XRD. During initial lithiation from open circuit potential to 0.7 V, no obvious change in XRD patterns could be observed (a-b-c, a'-b'-c', a"-b"-c"), suggesting that the potential plateau may be associated with the reduction of amorphous Sn oxide shell and formation of solid electrolyte interphase on the surface of the MSn_5 nanospheres. Reduction of Sn oxide and formation of SEI at potential above 0.7 V had been reported.[44, 45] During lithiation from 0.7 to 0.3 V (c-d, c'-d' c"-d"), XRD maintained unchanged but slightly shifted, demonstrating potential formation of an intermediate solid solution of $Li_xM_ySn_5$ (M = Fe, Co or FeCo, voltage ≥ 0.3 V). With further lithiation from 0.3 V to 0.01 V (d-e, d'-e', d"-e"), transition metals were extruded from MSn_5 compounds and Li with Sn yields a Li–Sn alloy phase. At the point of e (e' or e"), the peaks of XRD patterns became very weak and almost not visible, which might be attributed to the complete decomposition of MSn_5 (M = Fe, Co or FeCo) phase to form amorphous or nano-sized Li-Sn alloys. The reversible reactions mechanism during the first lithiation could be described as:

$$xLi + M_ySn_5 \rightarrow Li_xM_ySn_5 \text{ (M = Fe, Co or FeCo, 0.7- 0.3 V);} \quad (1)$$

$$zLi + Li_xM_ySn_5 \rightarrow Li_{x+z}Sn_5 + yM \text{ } (x + z \leq 22, \text{ 0.3-0.01 V);} \quad (2)$$

In the charge process, at the point of f, f', f" (0.65 V), weaker XRD diffraction peaks of $Li_xM_ySn_5$ appeared again (especially in f' and f''). Further delithiation to 1.5 V, the reformation of MSn_5 (M = Fe, Co or FeCo) peaks could be observed, which illustrated the high reversibility of lithiation/delithiation reaction. The reactions mechanisms during the delithiation could be expressed as follows:

$$Li_{x+z}Sn_5 + yM \rightarrow zLi + Li_xM_ySn_5 \text{ } (x + z \leq 22, \text{ voltage} \geq 0.65 \text{ V);} \quad (3)$$

$$Li_xM_ySn_5 \rightarrow xLi + M_ySn_5 \text{ (M = Fe, Co or FeCo, voltage} \geq 1.5 \text{ V);} \quad (4)$$

The lithiation/delithiation mechanism of $FeSn_5$, $Fe_{0.5}Co_{0.5}Sn_5$ and $CoSn_5$ nanospheres electrode proposed based on XRD are also supported by the Sn K-edge XAFS spectra taken during the first cycle at Li insertion to 0.01 V and Li removal to

1.5 V (**Fig. 4**c, **4**f, **4**i). Correspondingly, XAFS patterns at point e, e', e" (0.01 V) could be associated with the formation of a Li–Sn alloy phase.[46] Moreover, in the three electrodes, after the following full delithiation (g, g', g"), the phase could be indexed to the original tetragonal structure $FeSn_5$, $Fe_{0.5}Co_{0.5}Sn_5$, $CoSn_5$ in the P4/mcc space group, illustrating the complete reversibility of these three MSn_5 compounds.

Due to the large volume change, the morphology of MSn_5 also changed with lithiation/delithiation cycles. The uneven distribution of $FeSn_5$ nanoparticles could be clearly observed (**Fig. 5**a) after the first cycle, which were caused from massive volume change in lithium insertion/extraction, while $Fe_{0.5}Co_{0.5}Sn_5$, $CoSn_5$ could almost maintain the original morphology (**Fig. 5**c, **5**e). Moreover, the 3-4 nm of amorphous oxide shell on a single-crystalline intermetallic MSn_5 core became blurred or disappeared (**Fig. 5**b, **5**d, **5**f) after one cycle. These results showed the irreversible lithiation reaction of amorphous Sn based oxide shell. The EDS spectrum (**Fig. S2**) illustrates the ratios of Sn/Fe, Sn/Fe+Co, Sn/Co in $FeSn_5$, $Fe_{0.5}Co_{0.5}Sn_5$ and $CoSn_5$ nanocrystals still maintained to 7:1, 7:1 and 6:1 after one charge/discharge cycle.

The structure and composition stability of the $FeSn_5$, $CoSn_5$ and $Fe_{0.5}Co_{0.5}Sn_5$ nanocrystals after extended 100 cycles were also analyzed. From the TEM images, $FeSn_5$ anode material could still keep the morphology of nanospheres; however, they had a wide range of size with tens to hundreds of nanometers (**Fig. 6**a). However, the morphology of $CoSn_5$ anode significantly changed from the spherical to cubic structure (**Fig. 6**d). $Fe_{0.5}Co_{0.5}Sn_5$ nanocrystals had both cubic structure and small sphere nanoparticles after 100 cycles (**Fig. 6**g). Selected-area electron diffraction (SAED) patterns of the three compounds demonstrate that both cubic and sphere particles were in crystal structures (**Fig. 6**b, **6**e, **6**h). Further, EDS image (**Fig. 6**c) shows that Fe and Sn elements in $FeSn_5$ nanoparticles were completely separated, and only Fe was found in the TEM investigated region (Figure 6a). The separation of Fe from Sn and aggregation of Sn particles may result in quick capacity decline of $FeSn_5$ (Fig. 3d). On the contrary, Sn/Co with the ratio close to the 2:1~4:1 existed in $CoSn_5$ cubic particles (**Fig. 6**f). Similarly, all Fe, Co and Sn elements appeared in **Fig. 6**i where the cubic particle was Co-Sn alloy (**Fig. S3**) and small particles were Fe. These may be the reason why $Fe_{0.5}Co_{0.5}Sn_5$ could retain good cycling stability as $CoSn_5$ did.

To investigate the effect of transition metals on the thermodynamic property of MSn_5, the equilibrium potential of three MSn_5 compounds at different delithiation levels were measured using galvanostatic intermittent titration technique[47] by applying current pulse of 20 mA/g for 0.5 h and then relaxed for 4.0 h to reach quasi-equilibrium potentials. The delithiation equilibrium potentials of the $FeSn_5$, $Fe_{0.5}Co_{0.5}Sn_5$ and $CoSn_5$ compounds at different delithiation state (normalized capacity) are shown in **Fig. 7**a. As expected, the three compounds had similar equilibrium potential due to the same crystal structure and similar properties of Co and Fe. Three potential plateaus were clearly observed in all three compounds corresponding to successive phase change during delloying process. The equilibrium potentials of MSn_5 showed three plateaus between 0.0 V to 0.7 V, which could be assigned to the delithiation of Li from Li_xSn alloys and react with local M to form Li_xMSn_5 compounds. Further delithiation from 0.7 V to 1.2 V, the Li_xMSn_5 would change back to MSn_5. The equilibrium potential of three MSn_5 almost overlapped each other except of capacity at the second potential plateau at 0.65 V where $CoSn_5$ showed slightly higher capacity than $FeSn_5$ and $Fe_{0.5}Co_{0.5}Sn_5$ lay between them.

The reaction resistances are determined by dividing overpotential with pulse current in GITT measurement. **Fig. 7**b shows the evolution of reaction resistance during lithiation/delithiation of three MSn_5 compounds and the corresponding GITT curves are shown in **Fig. S4**. The reaction resistance of three compounds during charge and discharge also showed similar trend. The reaction resistance decreased in the beginning of lithiation, then stabilized but periodically changed with successive phase transformation and finally decreased again towards the end. Periodical changed in reaction resistance during the phase change was observed in graphite,[48] which was attributed to gradually increasing in diffusion length in each phase transformation process. The decrease in reaction resistance in initial and final lithiation could be due to the volume expansion reducing the interfacial resistance and increasing the conductivity of the compounds. In these three MSn_5 compounds, $CoSn_5$ showed the lowest lithiation reaction resistance, and $FeSn_5$ had the highest lithiation reaction resistance and $Fe_{0.5}Co_{0.5}Sn_5$ lay between them. The calculated resistances of $Fe_{0.74}Sn_5$ anode materials at 25%, 50% and 75% SOCs during lithiation were 4.5, 4.0 and 4.0 Ω g respectively, and $Co_{0.83}Sn_5$ nanospheres corresponding resistances were 3.6, 2.8 and 2.8 Ω g at 25%, 50% and 75% SOCs. As compared, the reaction resistances of $Fe_{0.35}Co_{0.35}Sn_5$ system during lithiation were 4.0, 3.6 and 3.2 Ω g. During delithiation, the reaction resistances of three compounds were similar. They increased in the beginning, stabilized afterwards and spiked towards the end.

Since the electrochemical impedance spectroscopy (EIS) could provide individual reaction resistances in the total reaction resistance determined by GITT, EIS was applied to these three compounds after being discharged to 0.3 V at 20 mA g^{-1} in the 5th cycle and being relaxed for 2 h shown in **Fig. 7**c. The EIS consisted of a depressed semicircle in the high frequency and slop line in the low frequency region. The high-frequency semicircle was related to interfacial (SEI and charge-transfer) resistances. The interface resistance of $FeSn_5$ was larger than $CoSn_5$ and $Fe_{0.5}Co_{0.5}Sn_5$ lay between them, which were in good agreement with the total reaction resistance measured using GITT. Based on the GITT and EIS results, the $FeSn_5$ anodes had higher reaction resistance, lower reversibility than $CoSn_5$ and $Fe_{0.5}Co_{0.5}Sn_5$ lay between them. The high reaction resistance and low reversibility of $FeSn_5$ might lead to separation of Fe to Sn and Sn aggregation, thus quickly capacity decay. $Fe_{0.5}Co_{0.5}Sn_5$ system could effectively tune the reaction resistance and cycling stability thus retained good cycling stability as $CoSn_5$ did, with high specific capacity due to the presence of Fe.

4. Conclusions

In conclusion, intermetallic MSn_5 (M=Fe, Co and FeCo) phase with the same structure, particle surface morphology and similar particle size distribution was synthesized using nanocrystal conversion chemistry method for comparison study on the mechanism of lithiation/delithiation, capacity decline and reaction kinetics. $Fe_{0.74}Sn_5$ has high capacity and $Co_{0.83}Sn_5$ has long cycling stability, while $Fe_{0.35}Co_{0.35}Sn_5$ anode can take both advantages of both high capacity of $Fe_{0.74}Sn_5$ and long cycle life of $Co_{0.83}Sn_5$, providing 736 mAh g^{-1} and maintaining 92.7% of initial capacity after 100 cycles with an average capacity loss of only 0.07% per cycle. The ex situ XRD and XAFS indicate MSn_5 (M=Fe, Co and FeCo) phase is almost completely reversible for the first charge/discharge cycle. Upon further charging /discharging to 100 cycles, Sn in $FeSn_5$ is gradually separated from Fe aggregated into large particle, resulting in quick capacity decay. However, Sn in $CoSn_5$ still alloys with Co although the ratio of Sn to Co decreases from 6:1 to 4:1, demonstrating a high cycling stability. The exceptional electrochemical property of $Fe_{0.5}Co_{0.5}Sn_5$ electrode is attributed to coexistence of Fe and Co-Sn. In addition, $Fe_{0.5}Co_{0.5}Sn_5$ also inherits the low reaction resistance of $CoSn_5$. The thorough understanding on the origins of excellent electrochemical performance of intermetallic MSn_5 (M=Fe, Co and FeCo) phase provides new opportunities for exploring other high capacity and long cycle life Sn-based anode materials.

Acknowledgements

This work is supported by the “Strategic Priority Research Program” of the Chinese Project Academy of Science, Grant No. XDA01020304, the National Natural Science Foundation of China (Grant No. 51371186), Ningbo 3315 International Team of Advanced Energy Storage Materials, Zhejiang Province Key Science and Technology Innovation Team (Grand No. 2013PT16), China Postdoctoral Science Foundation funded project (Grant No. 2013M541807) and Ningbo Natural Science Foundation (Grant No. 2014A610046).

Reference

1. B. Dunn, H. Kamath and J. M. Tarascon, *Science*, 2011, 334, 928-935.
2. J. Zhu, G. Zhang, X. Yu, Q. Li, B. Lu and Z. Xu, *Nano Energy*, 2014, 3, 80-87.
3. K. Amine, I. Belharouak, Z. Chen, T. Tran, H. Yumoto, N. Ota, S. T. Myung and Y. K. Sun, *Adv. Mater.* , 2010, 22, 3052-3057.
4. N. Mahmood, C. Z. Zhang, F. Liu, J. H. Zhu and Y. L. Hou, *Acs Nano*, 2013, 7, 10307-10318.

5. B. Liu, A. Abouimrane, M. Balasubramanian, Y. Ren and K. Amine, *The Journal of Physical Chemistry C*, 2014, 118, 3960-3967.
6. R. Mukherjee, R. Krishnan, T.-M. Lu and N. Koratkar, *Nano Energy*, 2012, 1, 518-533.
7. M. J. Armstrong, C. O'Dwyer, W. J. Macklin and J. D. Holmes, *Nano Res.*, 2014, 7, 1-62.
8. Z. Zhu, S. Wang, J. Du, Q. Jin, T. Zhang, F. Cheng and J. Chen, *Nano Lett.* , 2014, 14, 153-157.
9. M. G. Kim and J. Cho, *Adv. Funct. Mater.* , 2009, 19, 1497-1514.
10. B. Luo, B. Wang, X. Li, Y. Jia, M. Liang and L. Zhi, *Adv. Mater.* , 2012, 24, 3538-3543.
11. L. W. Ji, Z. K. Tan, T. Kuykendall, E. J. An, Y. B. Fu, V. Battaglia and Y. G. Zhang, *Energy Environ. Sci.* , 2011, 4, 3611-3616.
12. H. Li, Z. Wang, L. Chen and X. Huang, *Adv. Mater.* , 2009, 21, 4593-4607.
13. Y. Yu, L. Gu, C. Wang, A. Dhanabalan, P. A. van Aken and J. Maier, *Angew. Chem. Int. Ed.* , 2009, 48, 6485-6489.
14. A. D. W. Todd, P. P. Ferguson, J. G. Barker, M. D. Fleischauer and J. R. Dahn, *J. Electrochem. Soc.* , 2009, 156, A1034-A1040.
15. M. A. J.-M. Tarascon, *Nature*, 2001, 414, 359-367.
16. R. M. Gnanamuthu, Y. N. Jo and C. W. Lee, *J. Alloys Compd.* , 2013, 564, 95-99.
17. Q. Fan, P. J. Chupas and M. S. Whittingham, *Electrochem. Solid-State Lett.* , 2007, 10, A274-A278.
18. M. Chamas, P.-E. Lippens, J.-C. Jumas, K. Boukerma, R. Dedryvere, D. Gonbeau, J. Hassoun, S. Panero and B. Scrosati, *J. Power Sources* 2011, 196, 7011-7015.
19. U. G. Nwokeke, A. V. Chadwick, R. Alcantara, M. Alfredsson and J. L. Tirado, *J. Alloys Compd.* , 2011, 509, 3074-3079.
20. N. Tamura, Y. Kato, A. Mikami, M. Kamino, S. Matsuta and S. Fujitani, *J. Electrochem. Soc.* , 2006, 153, A2227-A2231.
21. X.-L. Wang, M. Feygenson, H. Chen, C.-H. Lin, W. Ku, J. Bai, M. C. Aronson, T. A. Tyson and W.-Q. Han, *J. Am. Chem. Soc.* , 2011, 133, 11213-11219.
22. X.-L. Wang, H. Chen, J. Bai and W.-Q. Han, *J. Phys. Chem. Lett.* , 2012, 3, 1488-1492.
23. Y. Zhu, Y. Xu, Y. Liu, C. Luo and C. Wang, *Nanoscale*, 2013, 5, 780-787.
24. A. A. a. G. Y. Benjamin Hertzberg, *J. Am. Chem. Soc.* , 2010, 132, 8548-8549.

25. J. Hassoun, G. A. Elia, S. Panero and B. Scrosati, *J. Power Sources* 2011, 196, 7767-7770.

26. N. Tamura, A. Fujimoto, M. Kamino and S. Fujitani, *Electrochim. Acta* 2004, 49, 1949-1956.

27. F.-S. Ke, L. Huang, B. C. Solomon, G.-Z. Wei, L.-J. Xue, B. Zhang, J.-T. Li, X.-D. Zhou and S.-G. Sun, *J. Mater. Chem.* , 2012, 22, 17511-17517.

28. P. P. Ferguson, D.-B. Le, A. D. W. Todd, M. L. Martine, S. Trussler, M. N. Obrovac and J. R. Dahn, *J. Alloys Compd.* , 2014, 595, 138-141.

29. C. M. Park, J. H. Kim, H. Kim and H. J. Sohn, *Chem. Soc. Rev.* , 2010, 39, 3115-3141.

30. H. Guo, H. Zhao, X. Jia, X. Li and W. Qiu, *Electrochim. Acta* 2007, 52, 4853-4857.

31. G. Saito, Y. Nakasugi, T. Yamashita and T. Akiyama, *Nanotechnology*, 2014, 25, 135603.

32. O. Mao and J. R. Dahn, *J. Electrochem. Soc.* , 1999, 146, 423-427.

33. M. R. Buck and R. E. Schaak, *Angew. Chem. Int. Ed.* , 2013, 52, 6154-6178.

34. M. R. Buck, J. F. Bondi and R. E. Schaak, *Nat Chem*, 2012, 4, 37-44.

35. Y. Vasquez, A. E. Henkes, J. Chris Bauer and R. E. Schaak, *J. Solid State Chem.* , 2008, 181, 1509-1523.

36. N. H. Chou and R. E. Schaak, *J. Am. Chem. Soc.* , 2007, 129, 7339-7345.

37. K. Hamaya, H. Itoh, O. Nakatsuka, K. Ueda, K. Yamamoto, M. Itakura, T. Taniyama, T. Ono and M. Miyao, *Phys. Rev. Lett.* , 2009, 102, 137204.

38. A. Vasil’ev, A. Bozhko, V. Khovailo, I. Dikshtein, V. Shavrov, V. Buchelnikov, M. Matsumoto, S. Suzuki, T. Takagi and J. Tani, *Phys. Rev. B*, 1999, 59, 1113.

39. W.-K. Hu, *J. Alloys Compd.* , 1998, 279, 295-300.

40. L. Xu, C. Kim, A. K. Shukla, A. Dong, T. M. Mattox, D. J. Milliron and J. Cabana, *Nano Lett.* , 2013, 13, 1800-1805.

41. L. Y. Beaulieu, S. D. Beattie, T. D. Hatchard and J. R. Dahn, *J. Electrochem. Soc.* , 2003, 150, A419-A424.

42. K. Kravchyk, L. Protesescu, M. I. Bodnarchuk, F. Krumeich, M. Yarema, M. Walter, C. Guntlin and M. V. Kovalenko, *J. Am. Chem. Soc.* , 2013, 135, 4199-4202.

43. G. Derrien, J. Hassoun, S. Panero and B. Scrosati, *Adv. Mater.* , 2007, 19, 2336-2340.

44. M. S. Park, G. X. Wang, Y. M. Kang, D. Wexler, S. X. Dou and H. K. Liu, *Angewandte Chemie*, 2007, 46, 750-753.

45. I. A. Courtney and J. R. Dahn, *J. Electrochem. Soc.* , 1997, 144, 2943-2948.

46. A. N. Mansour, S. Mukerjee, X. Q. Yang and J. McBreen, *J. Electrochem. Soc.* , 2000, 147, 869-873.

47. Y. Xu, Y. Zhu, Y. Liu and C. Wang, *Adv. Energy. Mater.*, 2013, 3, 128-133.

48. C. Wang, I. Kakwan, A. J. Appleby and F. E. Little, *J. Electroanal. Chem.* , 2000, 489, 55-67.

Figure and scheme captions

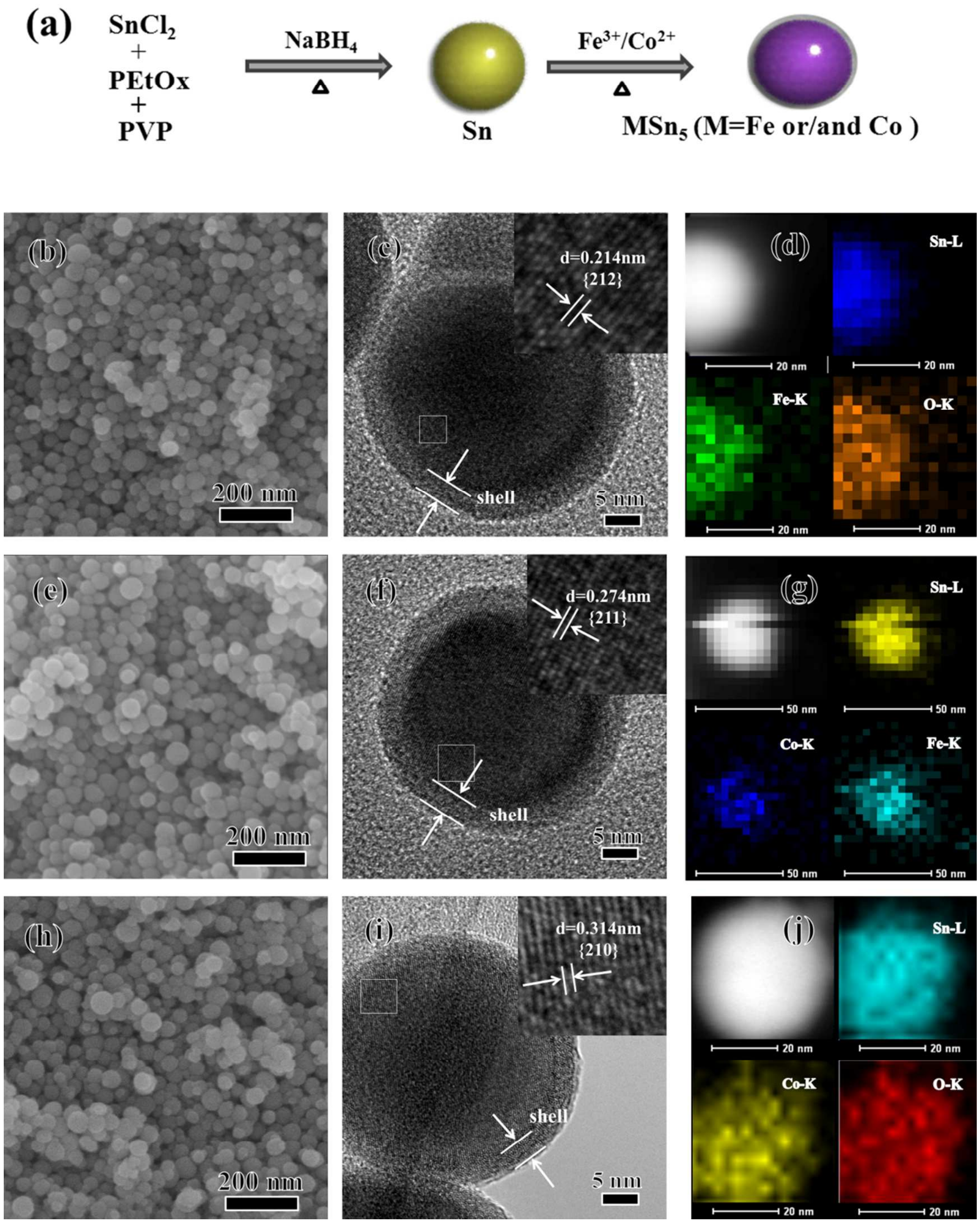

Fig. 1 a) Synthesis process for $FeSn_5$, $Fe_{0.5}Co_{0.5}Sn_5$ and $CoSn_5$ nanospheres; b, e, h) SEM; c, f, i) HRTEM; and d, g, j) STEM-EDS elemental mappings images of $FeSn_5$, $Fe_{0.5}Co_{0.5}Sn_5$ and $CoSn_5$ nanospheres

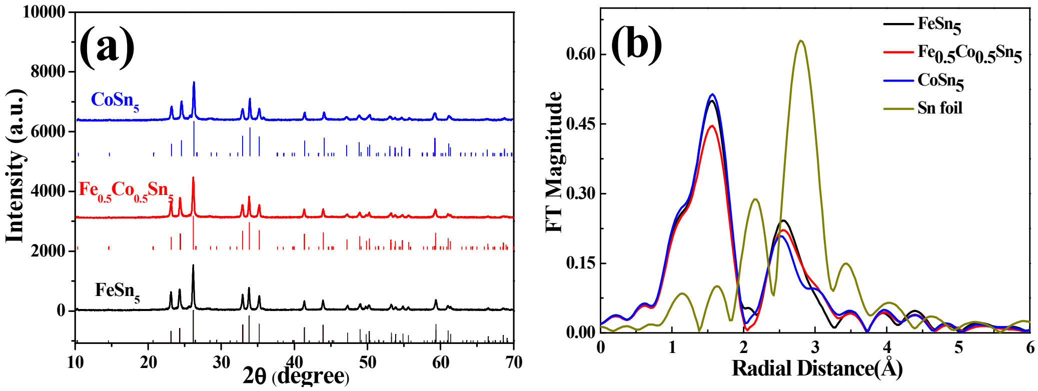

Fig. 2 a) Synchrotron XRD pattern of $FeSn_5$, $Fe_{0.5}Co_{0.5}Sn_5$ and $CoSn_5$ nanospheres; b) Synchrotron XAFS profile of the synthesized $FeSn_5$, $Fe_{0.5}Co_{0.5}Sn_5$ and $CoSn_5$ nanospheres.

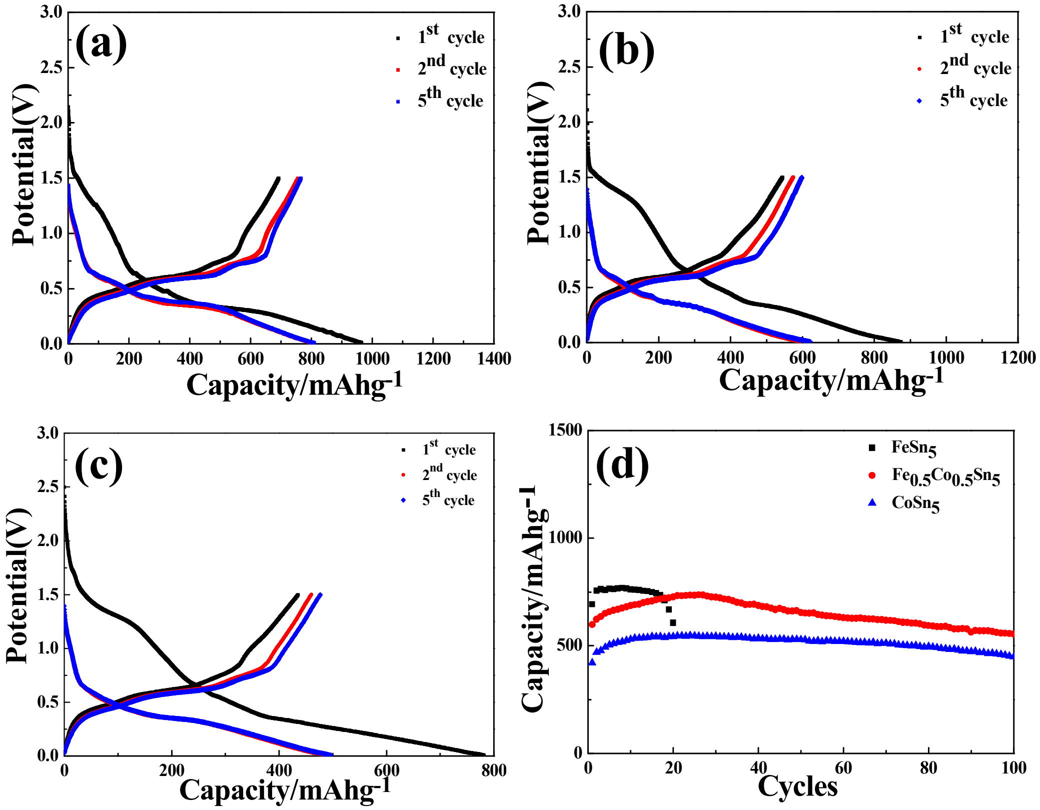

Fig. 3 a-c) Charge−discharge profiles of the half-cell with the $FeSn_5$, $Fe_{0.5}Co_{0.5}Sn_5$ and $CoSn_5$ nanospheres at the initial 1, 2 and 5 cycles at the current density of 0.05 C between 0.05-1.5 V. d) Reversible capacities of $FeSn_5$, $Fe_{0.5}Co_{0.5}Sn_5$ and $CoSn_5$ nanospheres as anodes in Li ion batteries at the current density of 0.05 C between 0.05-1.5 V.

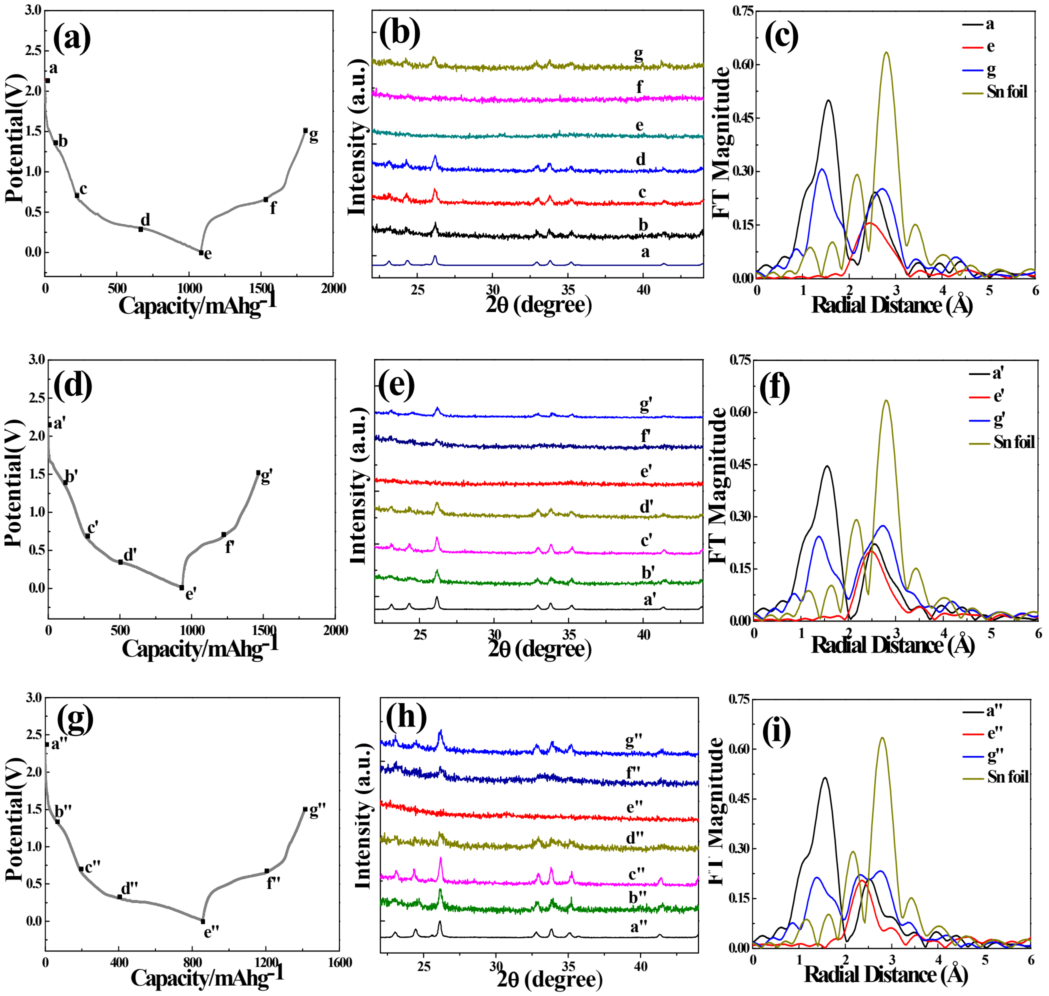

Fig. 4 a, d, g) Charge and discharge curves of the $FeSn_5$, $Fe_{0.5}Co_{0.5}Sn_5$ and $CoSn_5$ nanospheres electrode for the first cycle at a current density of 0.05 C; b, e, h) Synchrotron ex situ XRD patterns of at different potentials during discharge and charge processes of $FeSn_5$, $Fe_{0.5}Co_{0.5}Sn_5$ and $CoSn_5$ nanospheres electrode and c, f, i) the set of FTs of the Sn K-edge XAFS spectra taken during the first cycle.

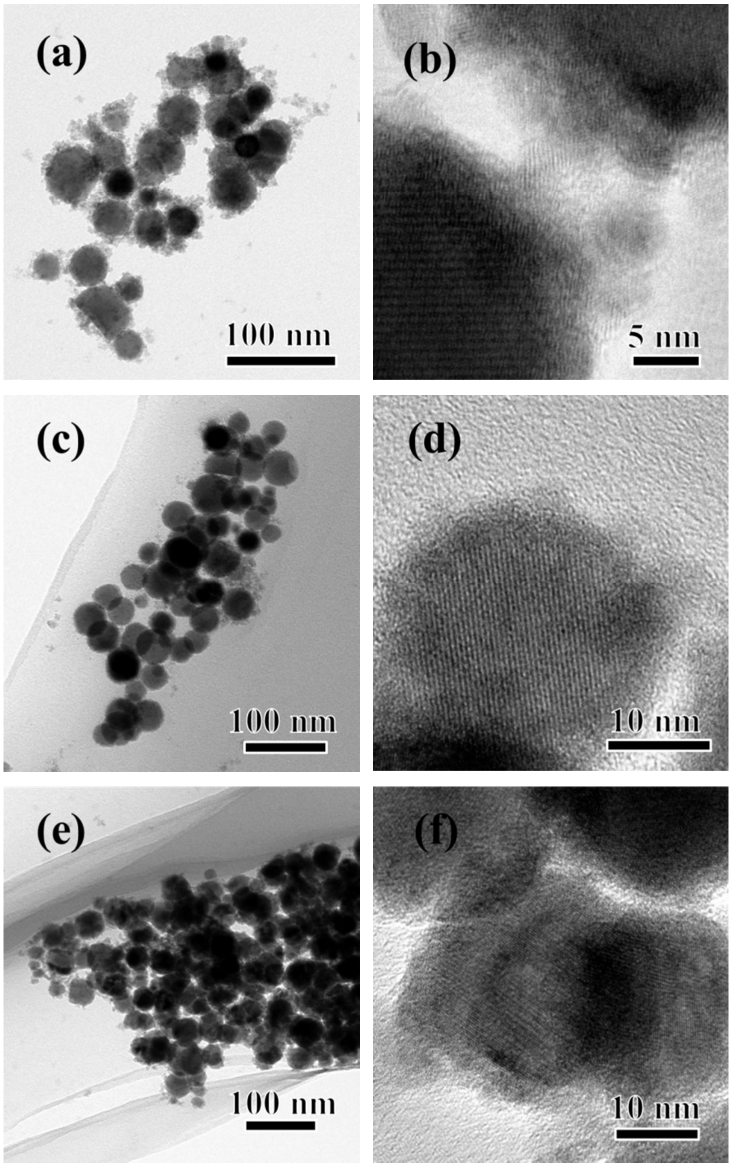

Fig. 5 a, c, e) TEM and b, d, f) HRTEM images of $FeSn_5$, $Fe_{0.5}Co_{0.5}Sn_5$ and $CoSn_5$ nanospheres after the first cycle

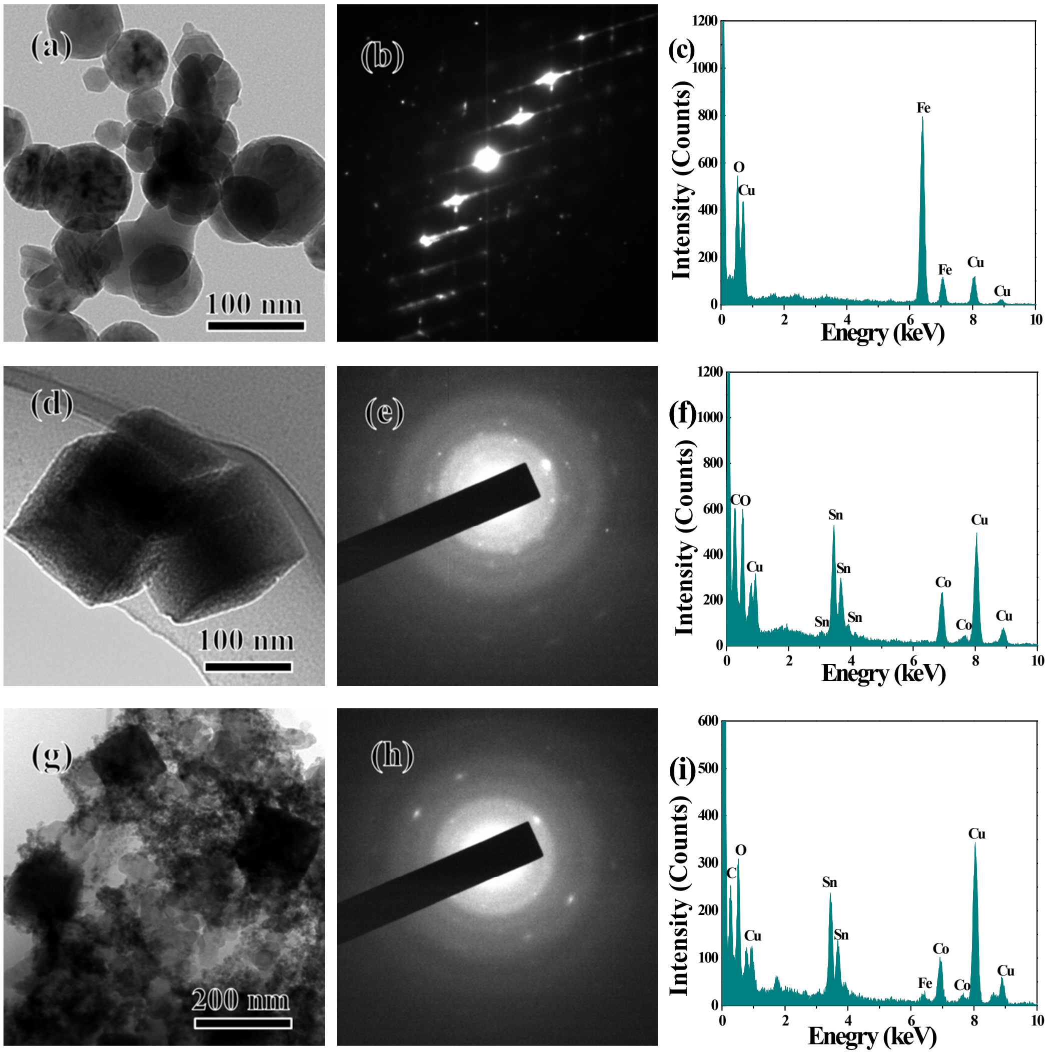

Fig. 6 a, d, g) TEM; b, e, h) ED and c, f, i) EDS images of $FeSn_5$, $CoSn_5$ and $Fe_{0.5}Co_{0.5}Sn_5$ nanospheres after 100 cycles at fully charged state (2.0 V)

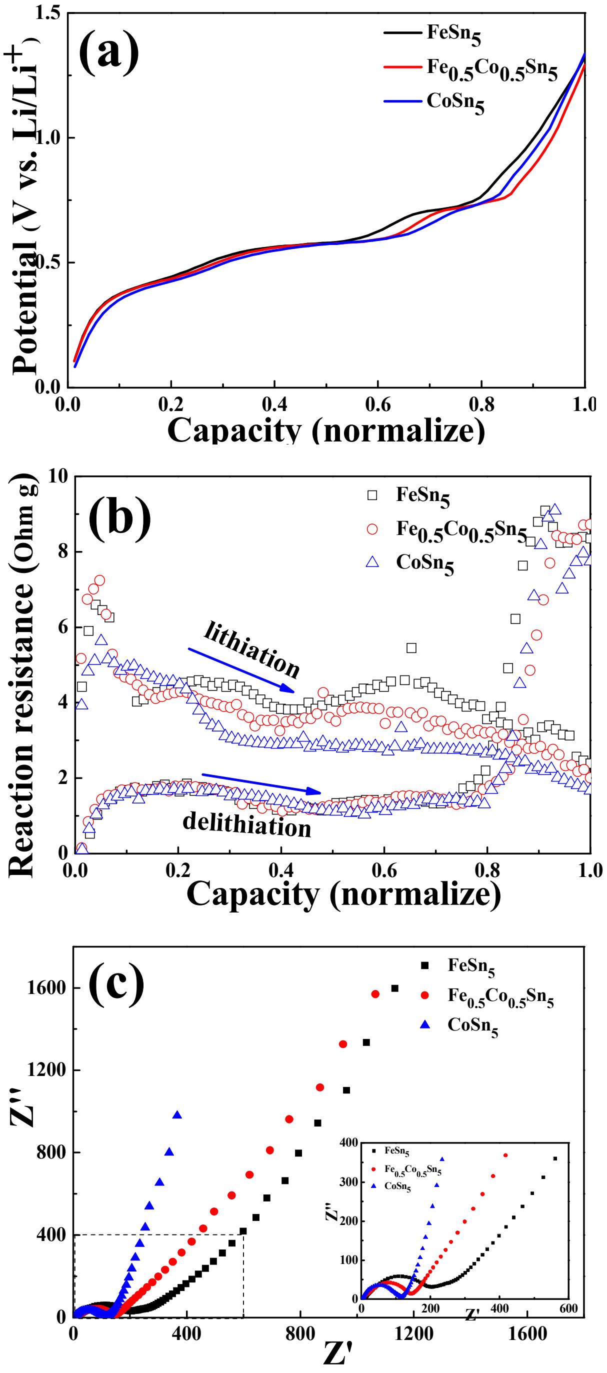

Fig. 7 a) Capacity normalized curves of FeSn$_5$, Fe$_{0.5}$Co$_{0.5}$Sn$_5$ and CoSn$_5$ nanospheres in the fifth cycle in the charge process and b) Comparison of reaction resistance of FeSn$_5$, Fe$_{0.5}$Co$_{0.5}$Sn$_5$ and CoSn$_5$ nanospheres and c) Electrochemical impedance spectroscopy of FeSn$_5$, Fe$_{0.5}$Co$_{0.5}$Sn$_5$ and CoSn$_5$ nanospheres after 5 charge/discharge cycles.

The same crystal structure, identical particle surface morphology and the similar particle size distribution of MSn_5 (M=Fe, Co and FeCo) phase are ideal for comparison on the electrochemical performance, reaction mechanism, thermodynamics and kinetics.